Ballistic-Diffusive Heat Conduction in Thin Films by Phonon Monte Carlo Method: Gray Medium Approximation Versus Phonon Dispersion

Han-Ling Li
Key Laboratory for Thermal Science and Power Engineering,
Department of Engineering Mechanics,
Ministry of Education,
Tsinghua University,
Beijing 100084, China
e-mail: li-hl16@mails.tsinghua.edu.cn

Junichiro Shiomi
Department of Mechanical Engineering,
The University of Tokyo,
7-3-1 Hongo, Bunkyo-ku,
Tokyo 113-8656, Japan
e-mail: shiomi@photon.t.u-tokyo.ac.jp

Bing-Yang Cao[1]
Key Laboratory for Thermal Science and Power Engineering of Department of Engineering Mechanics,
Ministry of Education,
Tsinghua University,
Beijing 100084, China
e-mail: caoby@tsinghua.edu.cn

The gray medium approximation treating all phonons with an averaged and representative mean-free-path (MFP) is an often used method in analyzing ballistic-diffusive heat conduction at nanoscale. However, whether there exists a reasonable value of the average MFP which effectively represents the entire spectrum of modal MFPs remains unclear. In this paper, phonon Monte Carlo (MC) method is employed to study the effects of the gray medium approximation on ballistic-diffusive heat conduction in silicon films by comparing with dispersion MC simulations. Four typical ways for calculating the average MFP with gray medium approximation are investigated. Three of them are based on the weighted average of the modal MFPs, and the remaining one is based on the weighted average of the reciprocals of the modal MFPs. The first three methods are found to be good at predicting effective thermal conductivity and heat flux distribution, but have difficulties in temperature profile, while the last one performs better for temperature profile than effective thermal conductivity and heat flux distribution. Therefore, none of the average MFPs can accurately characterize all the features of ballistic-diffusive heat conduction for the gray medium approximation. Phonon dispersion has to be considered for the accurate thermal analyses and modeling of ballistic-diffusive heat transport. Our work could be helpful for further understanding of phonon dispersion and more careful use of the gray medium approximation. [DOI: 10.1115/1.4048093]

Keywords: ballistic-diffusive heat conduction, phonon Monte Carlo, gray medium approximation, phonon dispersion

1 Introduction

The effective thermal management of electronic devices, which play an irreplaceable role in modern nanotechnology, is of great importance to their further miniaturization and integration. Nowadays, the characteristic length in these devices has reduced to nanoscale [1] and the power dissipation is becoming increasingly high. In 2018, the heat flux of hot spots in integrated circuits had been reported to be around 1000 W/cm^2 [2]. The high magnitude of power density and its highly nonuniform spatial distribution raise the average die temperature and produce local hot spots, impairing the reliability and lifetime [3]. Therefore, accurate thermal analyses are essential to evaluate the thermal design and find better designs to improve the performance of electronic devices.

Heat conduction is the primary way of cooling inside electronic devices and has received a great deal of recent attention. At macroscopic scale, heat conduction follows traditional Fourier's law, but when it comes to nanoscale, a growing number of experimental measurements have observed the breakdown of Fourier's law [4–10], motivating the study of the mechanism of non-Fourier heat conduction as well as new techniques which can well characterize such phenomena. A powerful approach to understand the thermal conduction is by investigating phonon transport, in which phonon mean-free-path (MFP), a property describing the distance the heat carrier can transmit thermal energy before being scattered, is a critical factor. Phonon ballistic transport is one of the main reasons for the failure of Fourier's law at nanoscale [11,12]. The strength of phonon ballistic transport generally can be described by $\mathrm{Kn} = l/L$, in which l denotes the phonon MFP and L the characteristic length of the system. When L is much larger than l, the phonon–phonon scattering is sufficient and all phonons travel diffusively, as a result of which Fourier's law is valid. However, as L becomes comparable to l or even smaller than l, phonons can directly arrive at the boundary without phonon–phonon scattering. Such a process is termed as ballistic transport and can invalidate Fourier's law. In electronic devices, usually some phonons are transported ballistically while others diffusively, the corresponding mechanism is ballistic-diffusive heat transport [13–15]. There are three typical features of ballistic-diffusive heat conduction: (1) size effect of thermal conductivity [16,17], which refers to the reduction of thermal conductivity as the length scale decreases; (2) boundary temperature jump [18], which refers to the difference between the boundary temperature and the phonon bath temperature as shown in Fig. 1(*a*); (3) boundary heat flux slip [19,20], which refers to the heat flux reduction observed near the lateral adiabatic boundaries as shown in Fig. 1(*b*). The intensities of these features increase with L decreasing, and a favorable thermal analysis method is expected to correctly capture the features.

Phonons normally have a wide range of frequency spectrum and their MFPs span several orders of magnitude, for example, from 1 nm to 100 μm in room temperature silicon [21], making it difficult to completely fathom phonon transport. Efforts have been devoted to building prediction models for the effective thermal conductivity that can take phonon dispersion into consideration [22–25]. The basic idea is to calculate the contributions of all phonon modes and sum them up. Numerical methods, such as phonon

[1]Corresponding author.

Contributed by the Heat Transfer Division of ASME for publication in the Journal of Heat Transfer. Manuscript received January 8, 2020; final manuscript received July 13, 2020; published online September 18, 2020. Assoc. Editor: Jennifer R. Lukes.

Monte Carlo (MC) which solves the frequency-dependent phonon Boltzmann transport equation (BTE) [26–32], are also widely used in the studies of ballistic-diffusive heat conduction. Recently, laser-based measurement techniques were employed to extract the phonon MFP spectra successfully [33–35]. Considering phonon dispersion is supposed to get the most accurate results, but it is mostly too complex and time-consuming. As a helpful simplification, the gray medium approximation, which assumes phonon properties to be frequency independent and averages the frequency-dependent phonon properties over the phonon population [28], has been extensively used. Under the condition of gray medium approximation, an averaged and representative MFP (l_{av}) can be utilized to outline phonon transport, facilitating the fast theoretical and numerical analyses of ballistic-diffusive heat conduction. Majumdar [36] developed a simple expression for the effective thermal conductivity of thin films as $k_{eff}/k_{bulk} = 1/(1+\frac{4}{3}\frac{l_{av}}{L})$ (k_{eff} and k_{bulk} denote the effective and bulk material thermal conductivity, respectively). Alvarez and Jou [37] derived an explicit prediction model of the thermal conductivity that fits experimental measurements. Hua and Cao [38–40] concluded that effective thermal conductivity of nanostructures can be written as $k_{eff}/k_{bulk} = 1/(1+\alpha\frac{l_{av}}{L})$ where α is the geometry factor determined by the geometrical shape and heating scheme such as the location of heat sources and sinks. This type of expression is also valid in radial heat conduction [41]. The gray medium approximation has also been adopted in the researches of boundary temperature jump and boundary heat flux slip. The former is discovered to be proportional to the MFP at the corresponding temperature [18,42], and models established by different methods [43–46] can readily estimate the jump value. The latter can be calculated by the Fuchs–Sondheimer solution as an analogy to electrons [47]. It is concluded that although phonon properties are simplified, gray medium approximation does not impair the major characteristics of ballistic transport and is efficient in mechanism investigations. However, it also has some limitations. For example, a traditional way to calculate the average MFP is

$$l_{av} = \frac{3k_{bulk}}{Cv_{av}} \tag{1}$$

but different ways of calculating the volumetric specific heat (C) and average group velocity (v_{av}) lead to different values of l_{av}. For silicon at 300 K, Chen [13] found that l_{av} is 40.9 nm calculated by Debye model, and it changes to 260.4 nm when considering dispersion. Jeong et al. [25] presented $l_{av} = 115$ nm by extracting the average MFP from the measured thermal conductivity. Maznev et al. [9] suggested that the representative MFP should be about 0.5–1 μm according to the direct measurement of nondiffusive thermal transport. Furthermore, the gray medium approximation is reported to fail to predict the temperature accurately [48,49]. In fact, the practicality of the gray medium approximation is highly dependent on the choice of the average MFP, and detailed and in-depth study on the influence of using an average MFP on thermal analyses and whether there exists a reasonable choice of the value is needed.

In the present work, we use phonon tracing MC method to study the ballistic-diffusive heat conduction in silicon thin films, focusing on comparisons between phonon dispersion and gray medium approximation. By taking the results considering phonon dispersion as a benchmark, four typical ways of calculating the average MFP in gray medium approximation are compared. The first three methods can be classified as being based on the weighted average of the MFPs, while the last one is based on the weighted average of the reciprocals of the MFPs. These methods are found to have their own drawbacks, and there does not exist an appropriate choice of the average MFP that can exactly reflect all the features of ballistic-diffusive heat conduction. This can be interpreted in terms of a tradeoff between the accuracy of

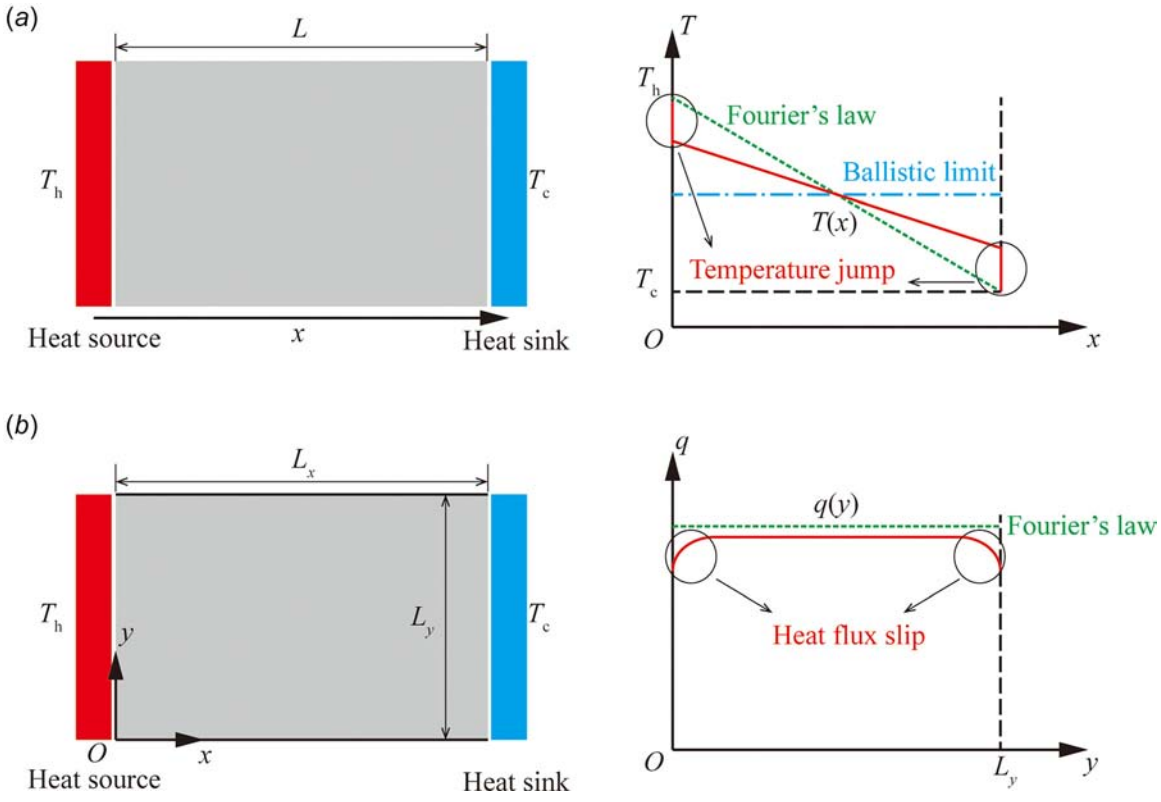

Fig. 1 Schematics of ballistic-diffusive heat conduction in thin films [20]: (*a*) cross-plane heat conduction and boundary temperature jump; (*b*) in-plane heat conduction and boundary heat flux slip

cross section-related thermal properties and that of volume-related thermal properties in gray medium approximation.

2 Methodology

2.1 Phonon Monte Carlo Method. The phonon BTE with relaxation time approximation in steady-state is given by [50]

$$\mathbf{v}_{p,\omega} \cdot \nabla f_{p,\omega} = \frac{f^0_{p,\omega} - f_{p,\omega}}{\tau_{p,\omega}} \tag{2}$$

where $\mathbf{v}_{p,\omega}$, $f^0_{p,\omega}$, $f_{p,\omega}$ and $\tau_{p,\omega}$ denote the mode-dependent group velocity vector, the phonon distribution function, the Bose–Einstein distribution in equilibrium and the relaxation time, respectively. Equation (2) is hard to be solved directly because it involves variables in both real and momentum space [14]. Instead, phonon MC method, which is especially useful for complex geometric structures and readily incorporates different scattering events, has been broadly employed. In this paper, we utilize phonon tracing MC method, which assumes that the properties of different phonon bundles are independent and each phonon bundle can be tracked individually. Details of the gray medium phonon tracing MC simulation can be found in Refs. [38], [39], and [43].

When considering phonon dispersion, the main difference is that phonon bundles emitted from phonon baths will have different properties, and their properties will be redetermined after phonon–phonon scattering. The key point is to calculate the distribution function from which phonon bundles are drawn. An energy-based variance-reduced technique reported in Ref. [30] is adopted, then the emitting distribution for phonon–phonon scattering can be written as $(e^0 - e^0_{T_{eq}})D/\tau(\omega,p,T)d\,\omega$, in which $e^0 = \hbar\,\omega f^0$, D denotes the volumetric density of state and T_{eq} is an artificially prescribed reference temperature. For small temperature differences, $e^0 - e^0_{T_{eq}}$ can be simplified as $(T - T_{\rm eq})(de^0_{T_{\rm eq}}/dT)$, and the emitting distribution is linearized as $(T - T_{\rm eq})(de^0_{T_{\rm eq}}/dT)Dd\,\omega/\tau(\omega,p,T_{eq})$ [31]. It should be noted that this distribution does not depend on $(T - T_{eq})$ once normalized and $(de^0_{T_{\rm eq}}/dT)D = C_{p,\omega}$ where $C_{p,\omega}$ denotes the modal specific heat. Thus, the probability of drawing a phonon bundle at polarization p and frequency ω after phonon–phonon scattering is

$$W_{\rm ph-ph} = \frac{C_{p,\omega}v_{p,\omega}/l_{p,\omega}}{\sum_p \int_\omega (C_{p,\omega}v_{p,\omega}/l_{p,\omega})d\omega}d\omega \tag{3}$$

in which $l_{p,\omega}$ is the modal MFP. For phonon bundles emitted from phonon baths, a similar derivation is conducted and the probability function is

$$W_{\rm ph-bnd} = \frac{C_{p,\omega}v_{p,\omega}}{\sum_p \int_\omega C_{p,\omega}v_{p,\omega}d\omega}d\omega \tag{4}$$

Compared to Eq. (4), the term $l_{p,\omega}$ in Eq. (3) is closely related to the different ways of generating new phonons between phonon–phonon scattering and phonon-boundary scattering. For phonon–phonon scattering, the probability function is calculated based on the contribution of each phonon mode to the pseudo-energy, while for phonon-boundary scattering based on their contributions to heat flux. After getting Eqs. (3) and (4), phonon tracing MC that considers phonon dispersion can be realized by extending the gray medium MC program [26]. In practice, the integrals over frequency are converted into the sums of many tiny intervals. It is worth noting that how to define temperature in ballistic-diffusive heat conduction remains to be controversial [13,51]. In this paper, the local equivalent equilibrium temperature which is a representation of the average energy of all phonons around a local postion is used [13,39,52]. It is equivalent to the equilibrium temperature of those phonons if they redistribute adiabatically to an equilibrium state, and is able to obtain results which agree well with those of Fourier's law when the system scale is large enough [53].

The phonon dispersion can be described by experiments [54], theoretical models [23] or first-principle calculations [55]. For silicon, the explicit Brillouin zone boundary condition (BZBC) model is selected since it reproduces the experimental data over the first Brillouin zone [24]. The dispersion relations for longitudinal (subscript "L") and transverse (subscript "T") phonon branches are

$$\omega_{\rm L} = v_{0,\rm L}\kappa_{\rm m}\kappa^* + (\omega_{\rm m,L} - v_{0,\rm L}\kappa_{\rm m})\kappa^{*2} \tag{5a}$$

$$\omega_{\rm T} = v_{0,\rm T}\kappa_{\rm m}\kappa^* + (3\omega_{\rm m,T} - 2v_{0,\rm T}\kappa_{\rm m})\kappa^{*2} + (v_{0,\rm T}\kappa_{\rm m} - 2\omega_{\rm m,T})\kappa^{*3} \tag{5b}$$

where $\kappa^* = \kappa/\kappa_{\rm m}$ is a dimensionless wave number, $\kappa_{\rm m} = 2\pi/a$ is the wave number at the edge of the first Brillouin zone, $\omega_{\rm m}$ is the upper limit of the angular frequency and v_0 is the group velocity at the low-frequency limit ($\kappa \to 0$). The first Brillouin zone is often assumed to be isotropic, which means the dispersion curves are identical in any wavevector direction. At room temperature ($T = 300$ K), experimental data in the [100] direction of silicon gives [24]: $a = 0.543$ nm, $\omega_{\rm m,L} = 210k_{\rm B}/\hbar$ rad/s, $\omega_{\rm m,T} = 570k_{\rm B}/\hbar$ rad/s, $v_{0,\rm L} = 8480$ m/s, and $v_{0,\rm T} = 5860$ m/s. Relaxation times are also required to carry out the dispersion MC. In this paper, the impurity scattering (I) and three phonon scattering (3 ph) in silicon are considered, and they are additive according to the Matthiessen's rule: $\tau_j^{-1} = \tau_{I,j}^{-1} + \tau_{\rm 3ph,j}^{-1}$ for $j = T$ (transverse), L (longitudinal). The impurity relaxation time can be expressed as (Rayleigh regime): $\tau_{I,j} = B_{I,j}(\omega)\omega^4$, and the usual N (normal) and U (umklapp) relaxation times for different polarization modes are: $\tau_{\rm 3ph,L}^{-1} = B_L\omega^2T^3$, $\tau_{\rm 3ph,T}^{-1} = \tau_{N,T}^{-1} + \tau_{U,T}^{-1}$ with

$$\tau_{N,T}^{-1} = \begin{cases} B_{N,T}\omega T^4, & \text{for } \omega < \omega_{1/2,T} \\ 0, & \text{for } \omega > \omega_{1/2,T} \end{cases}$$

and

$$\tau_{U,T}^{-1} = \begin{cases} 0, & \text{for } \omega < \omega_{1/2,T} \\ B_{U,T}\dfrac{\omega^2}{\sinh(\hbar\omega/k_{\rm B}T)}, & \text{for } \omega > \omega_{1/2,T} \end{cases}$$

[56]. B_I, B_L, $B_{N,T}$ and $B_{U,T}$ are the relaxation time parameters given in literature [24]. The modal MFP equals to the product of modal group velocity and modal relaxation time, $l_{p,\omega} = v_{p,\omega}\tau_{p,\omega}$. The bulk material thermal conductivity predicted by the BZBC model is $k_{\rm bulk} = \frac{1}{3}\sum_p \int_\omega C_{p,\omega}v_{p,\omega}l_{p,\omega}d\omega = 143.1\,{\rm W/(m\cdot K)}$. The reason why it is slightly lower than the textbook value ($150\,{\rm W/(m\cdot K)}$) is the neglect of the contribution of optical phonons. The MC simulation with BZBC model is able to reproduce the experimental results of thermal conductivity, which will be shown in Sec. 3.

2.2 Average MFP. Four different methods to define the average MFP denoted by $l_{\rm av,1}$, $l_{\rm av,2}$, $l_{\rm av,3}$, and $l_{\rm av,4}$ will be introduced and compared in this section. The first two are both obtained by Eq. (1), but the values of the bulk material thermal conductivity, specific heat, and average group velocity are different. The most conventional model for predicting the specific heat is Debye's theory, which gives $C(T) = 9\frac{\rho R}{M}\left(\frac{T}{\Theta_{\rm D}}\right)^3 \int_0^{\Theta_{\rm D}/T} \xi^4 e^\xi/(e^\xi - 1)^2 d\xi$ and $\frac{1}{v_{\rm av,0}^3} = \frac{1}{3}(\frac{1}{v_{0,\rm L}^3} + \frac{2}{v_{0,\rm T}^3})$. Here, ρ, R, M, and $\Theta_{\rm D}$ denote the density, universal gas constant, molar mass, and Debye temperature, respectively. For silicon at room temperature, it is derived that

$C_1/\rho = 715\,\mathrm{J/(kg\cdot K)}$ and $v_{\mathrm{av},1} = 6375\,\mathrm{m/s}$. Thus, we have $l_{\mathrm{av},1} = (3k_{\mathrm{bulk}}/C_1 v_{\mathrm{av},1}) = 40.4\,\mathrm{nm}$, which is the textbook value of the MFP for silicon at 300 K [43,56]. However, Debye specific heat does not distinguish the contribution of acoustic phonons and optical phonons, of which the latter contribute very little to thermal conductivity since their group velocities are close to zero. In fact, optical phonons are customarily ignored in heat conduction. In addition, the elastic wave approximation is bound to overestimate the average group velocity. Therefore, $l_{\mathrm{av},1}$ is an underestimated average MFP, which will reduce the size effect and over-predict the effective thermal conductivity.

In practice, it is more reasonable to only include the specific heat of acoustic phonons and calculate the average group velocity by the modal specific heat, that is $C_2 = \sum_{p=1}^{3}\int_0^{\omega_{\max}} C_{p,\omega}d\omega$ and $v_{\mathrm{av},2} = \left((\sum_p \int_0^{\omega_{\max}} C_{p,\omega}v_{p,\omega}d\omega)/(\sum_{p=1}^{3}\int_0^{\omega_{\max}} C_{p,\omega}d\omega)\right)$ [57]. Based on the BZBC model, we have $C_2/\rho = 424\,\mathrm{J/(kg\cdot K)}$ and $v_{\mathrm{av},2} = 2463\,\mathrm{m/s}$. The result that C_2 is nearly two-thirds of C_1 accords with the report that about one-third of the specific heat is due to optical phonons in room-temperature silicon [13], verifying the BZBC model. In this way, the average MFP is calculated as $l_{\mathrm{av},2} = (3k_{\mathrm{bulk}}/C_2 v_{\mathrm{av},2}) = 175.5\,\mathrm{nm}$. By rewriting the formula for $l_{\mathrm{av},2}$ as

$$l_{\mathrm{av},2} = \frac{\sum_p \int_{0^{\omega}\max C_{p,\omega}} v_{p,\omega}l_{p,\omega}d\omega}{\sum_p \int_{0^{\omega}\max C_{p,\omega}} v_{p,\omega}d\omega} \tag{6}$$

It can be interpreted as a weighted average of the modal MFPs where the weighting coefficient is fixed as $C_{p,\omega}v_{p,\omega}$. Thanks to the more careful treatment with phonon dispersion, the effective thermal conductivity based on $l_{\mathrm{av},2}$ has a closer agreement with dispersion results than $l_{\mathrm{av},1}$ [58]. However, when there is ballistic transport, the size effect on different phonon modes is different, making the contributions of different phonon modes to the thermal conductivity vary with the system length. The weighting coefficient of $l_{\mathrm{av},2}$ is based on the modal contributions in bulk material, thus it cannot reflect this change.

To overcome this drawback, a method to extract the average MFP by fitting the size-dependent thermal conductivity is proposed. When considering phonon dispersion, a robust model of the varied effective thermal conductivity is $k_{\mathrm{eff}} = \frac{1}{3}\sum_p \int_\omega C_{p,\omega}v_{p,\omega}l_{p,\omega}F(p,\omega)d\omega$ where $F(p,\omega)$ denotes the boundary scattering function [22]. Previous studies [28,29,57,58] have demonstrated that the effective thermal conductivities obtained by this model have a similar variation trend with the prediction of the gray medium models, so an average MFP can be extracted by using a gray medium model to fit the varied effective thermal conductivity. For silicon films, Majumdar's model for cross-plane heat conduction [36] is employed to calculate $F(p,\omega)$ and fit the dispersion results, then we have $l_{\mathrm{av},3} = 393.7\,\mathrm{nm}$. The gray medium approximation using $l_{\mathrm{av},3}$ ought to have the best performance in the prediction of the effective thermal conductivity. The validity of the fitting will be verified by the results in Sec. 3. It is worthy of note that $l_{\mathrm{av},3}$ is still a weighted average of the MFPs with the weighting coefficient being implicit.

In addition to averaging based on the contribution of thermal conductivity, another kind of the average MFP can be defined from the point of temperature. Just like photons, the equivalent equilibrium temperature of phonons is associated with the density of local emitted power by $dQ_e/dV = 4\varepsilon\sigma_{\mathrm{Phonon}}T^4$ under the gray medium approximation [43]. Here, $\varepsilon = (l_{\mathrm{av}})^{-1}$ and σ_{Phonon} denote the phonon absorption coefficient [36] and phonon Stefan–Boltzmann constant [59], respectively. When considering phonon dispersion, the relation is $dQ_e/dV = \sum_p \int_0^{\omega_{\max}} \varepsilon_{p,\omega}e_{p,\omega}(T)d\omega$ where $\varepsilon_{p,\omega} = (l_{p,\omega})^{-1}$ is the modal phonon absorption coefficient and $e_{p,\omega}(T)$ the modal phonon emissive intensity. An average absorption coefficient is set to satisfy $\sum_p \int_0^{\omega_{\max}} \varepsilon_{p,\omega}e_{p,\omega}(T)d\omega = \varepsilon_{\mathrm{av}}\sum_p \int_0^{\omega_{\max}} e_{p,\omega}(T)d\omega$, then the average MFP can be defined as $l_{\mathrm{av},4} = (\varepsilon_{\mathrm{av}})^{-1} = [\left(\sum_p \int_0^{\omega_{\max}} (l_{p,\omega})^{-1}e_{p,\omega}(T)d\omega\right)/\left(\sum_p \int_0^{\omega_{\max}} e_{p,\omega}(T)d\omega\right)]^{-1}$. For small temperature differences, $e_{p,\omega}(T) \propto C_{p,\omega}v_{p,\omega}$ [36], and the expression is converted to

$$l_{\mathrm{av},4} = \left[\frac{\sum_p \int_0^{\omega_{\max}} (l_{p,\omega})^{-1}C_{p,\omega}v_{p,\omega}d\,\omega}{\sum_p \int_0^{\omega_{\max}} C_{p,\omega}v_{p,\omega}d\,\omega}\right]^{-1} \tag{7}$$

According to the BZBC model, it is derived that $l_{\mathrm{av},4} = 43.2\,\mathrm{nm}$, which happens to be almost the same with the value of $l_{\mathrm{av},1}$ because of the particular dispersion relation of silicon. Ignoring the coincidence, $l_{\mathrm{av},4}$ is expected to have an advantage in predicting the temperature over other methods. The difference between the values of $l_{\mathrm{av},3}$ and $l_{\mathrm{av},4}$ suggests that there would be a contradiction between the accuracy of the effective thermal conductivity and the temperature, which will be displayed and discussed in detail in Sec. 3.

3 Results and Discussion

To examine the performance of the four ways to calculate the average MFP, cross-plane and in-plane heat conduction in silicon films shown in Fig. 1 are simulated with gray-medium approximation and phonon dispersion in this section. The films are heated by two heat baths with different temperatures, phonons will travel from the hot bath to the cold one, producing heat flow. During their travel, they will suffer phonon–phonon scattering and phonon–boundary scattering. The two cases are chosen not only for the fact that they can exhibit the features of ballistic-diffusive heat conduction comprehensively, but also considering the feasibility of using dispersion MC as a benchmark. More importantly, a more general heat conduction problem can be viewed in some extend as the composition of the two simple cases [38]. In present MC simulations, the bath temperatures are set to be $T_h = 305\,\mathrm{K}$ and $T_c = 295\,\mathrm{K}$, and phonon dispersion at 300 K is used. The effective thermal conductivity is defined as $k_{\mathrm{eff}} = ((q/L)/T_h - T_c)$. For in-plane heat conduction, the focus is on the impact

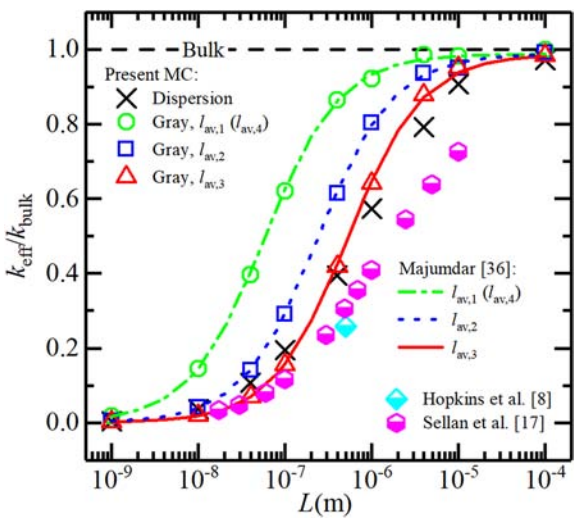

Fig. 2 Effective thermal conductivity varying with the film length (*L*) in cross-plane heat conduction. The model comes from Ref. [36], the experimental and other numerical results come from Refs. [8] and [17].

of the lateral boundaries, so the characteristic length is the film lateral length (L_y), and L_x is set to be large enough to neglect the size effect in the temperature difference direction. The lateral boundaries are set to be diffusive to generate an evident size effect and boundary heat flux slip. The numbers of simulated phonon bundles are 2×10^6 for the cross-plane case and 2×10^8 for the in-plane case. They are large enough to suppress the random error. All results shown below are normalized as $X = x/L$, $Y = y/L_y$, $T^* = ((T - T_c)/(T_h - T_c))$, and $q^* = q/q_{Fourier}$, in which $q_{Fourier}$ is the heat flux predicted by Fourier's law and is independent of the y coordinate.

3.1 Cross-Plane Heat Conduction. The ratios of the effective thermal conductivity to the bulk material value obtained by dispersion MC, as well as those of the gray medium MC using different values of the average MFP, are shown in Fig. 2. Since the values of $l_{av,1}$ and $l_{av,4}$ are almost the same, their results are coincident. When $L = 100\,\mu$m, all simulated results are close to the bulk material value and phonons are in diffusive regime (Fourier's law). As L decreases, no matter considering phonon dispersion or using the gray medium approximation, the simulated effective thermal conductivities gradually decrease, indicating the enhancement of ballistic transport. But for the same L, the size effect of the effective thermal conductivity is different for different simulation schemes. Take $L = 1\,\mu$m as an example, the most remarkable reduction is predicted by dispersion MC ($k_{eff}/k_{bulk} = 0.57$), followed by $l_{av,3}$ (0.64), $l_{av,2}$ (0.80), and $l_{av,1}$ (0.92). When L decreases to 1 nm, nearly all phonons are in ballistic regime (Casimir limit) and the corresponding effective thermal conductivities approach 0. Expectedly, the gray medium approximation is capable of reflecting the size effect of thermal conductivity qualitatively, but different values of the average MFP produce significantly different quantitative results. To check the accuracy of the MC simulations, experimental results in Ref. [8] and simulation results in Ref. [17] are illustrated in Fig. 2 too. It can be seen that results by phonon dispersion or using $l_{av,3}$ as the average MFP have the best consistency with previous experiment and

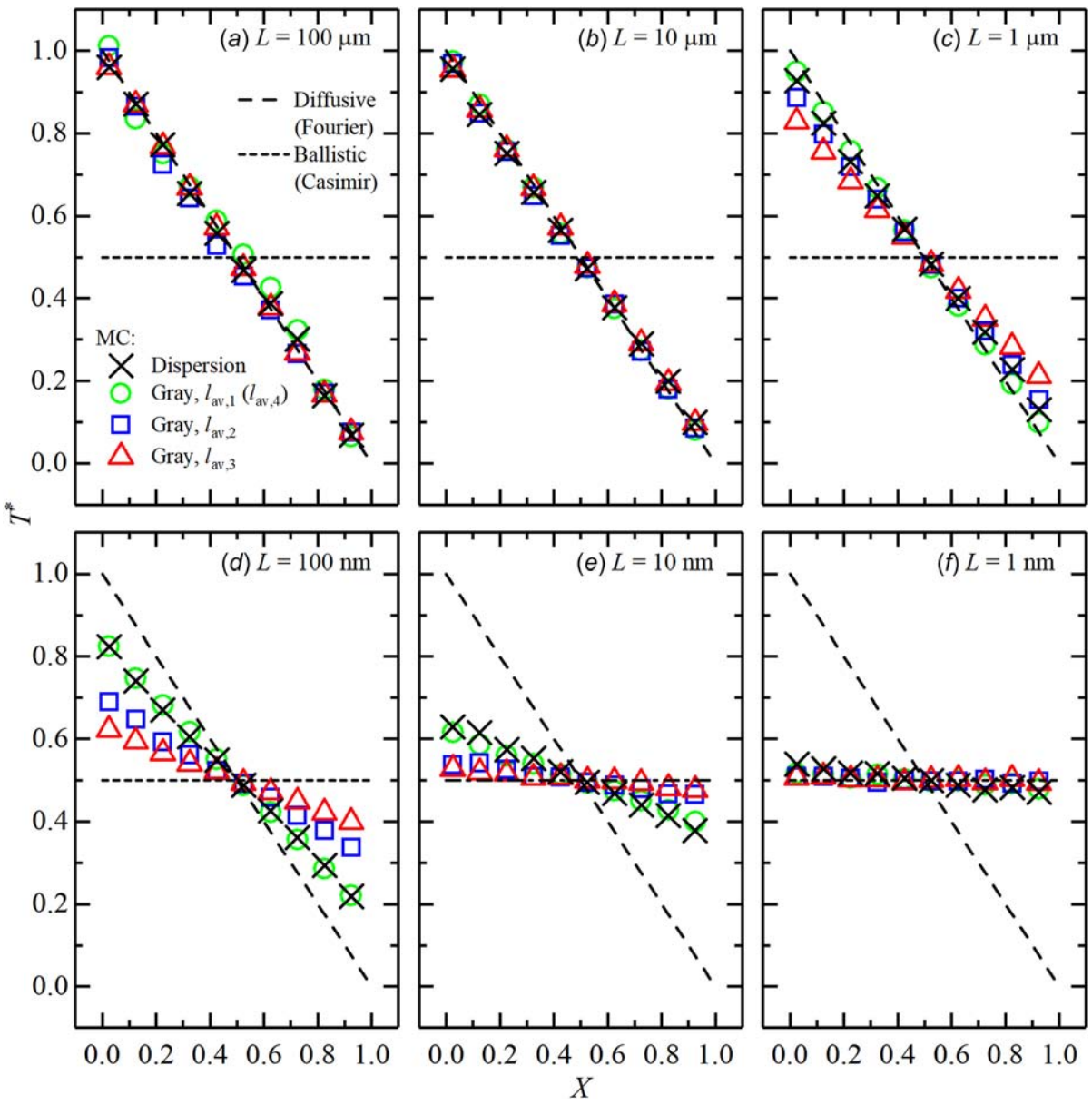

Fig. 3 Temperature distribution varying with the film length (L) in cross-plane heat conduction. "Diffusive" refers to diffusive limit, the corresponding temperature distribution follows Fourier's law. "Ballistic" refers to the ballistic limit, and the corresponding temperature is a constant inside the film.

simulation, followed by those using $l_{av,2}$ and the worst is $l_{av,1}$ ($l_{av,4}$). In addition, theoretical predictions based on Majumdar's model [36] are also given in Fig. 2. The acceptable agreement between the solid line and the cross symbols verifies the validity of fitting the dispersion results by Majumdar's model with $l_{av,3}$. To accurately predict the effective thermal conductivity, $l_{av,3}$ seems to be the better one.

However, when it comes to the temperature distribution, the conclusion is just the opposite. The temperature distributions of different film lengths are illustrated in Fig. 3 where the results in diffusive limit and ballistic limit are also depicted. Similar to the effective thermal conductivity, when $L = 100\,\mu$m, the temperature profiles look like the prediction of Fourier's law and there are no boundary temperature jumps. As L decreases, all simulations exhibit that the temperature profiles gradually deviate from the diffusive prediction and the boundary temperature occurs, but the degree of deviation and temperature jump values are different. For instance, at $L = 100$ nm, the results of phonon dispersion and $l_{av,1}$ ($l_{av,4}$) have the minimum deviations, and the corresponding dimensionless boundary temperature jumps are less than 0.2. For those of $l_{av,2}$ and $l_{av,3}$, the deviations raise and the corresponding temperature jump values are about 0.3 and 0.4, respectively. When it comes to $L = 1$ nm, all MC simulations predict the almost horizontal temperature profiles and the boundary temperature jumps are close to the maximum value (0.5) in ballistic limit. Comparing the gray medium MC to the dispersion MC, it is the result of $l_{av,1}$ ($l_{av,4}$) that has the best accuracy in temperature distribution on all scales while using $l_{av,2}$ or $l_{av,3}$ results in certain discrepancies in the intermediate scales ($L = 1$ μm, 100 nm, 10 nm). From the point of the temperature, $l_{av,4}$ appears to be the better choice. Combining the results of Figs. 2 and 3, it is found that the gray medium approximation cannot accurately predict the effective thermal conductivity and the temperature distribution at the same time.

The performance of different average MFPs is strongly related to their calculation methods. The effective thermal conductivity in ballistic-diffusive conduction is calculated by heat flux, which is a cross section-related thermal property. As a contrast, the equivalent equilibrium temperature is derived from the local emitted power density, which is a volume-related thermal property. An average method cannot take care of the cross section-related and volume-related thermal properties simultaneously. Consequently, the average method based on the modal contributions of the thermal conductivity ($l_{av,3}$) predicts effective thermal conductivities better than temperatures, while the method based on the modal contribution of the emitted power density ($l_{av,4}$) is preferable to predict the temperature. A good value of the average MFP is supposed to calculate both the thermal conductivity and the temperature distribution accurately on all scales, but it is extremely hard to find such a value owing to the natural limitation of the gray medium approximation. It should be noted that although there are other temperature definitions for nonequilibrium heat conduction [29], since they are all based on some kinds of volumetric energy density, the average MFP based on temperature is expected to always have difficulty in accurate predicting the cross section-related thermal properties.

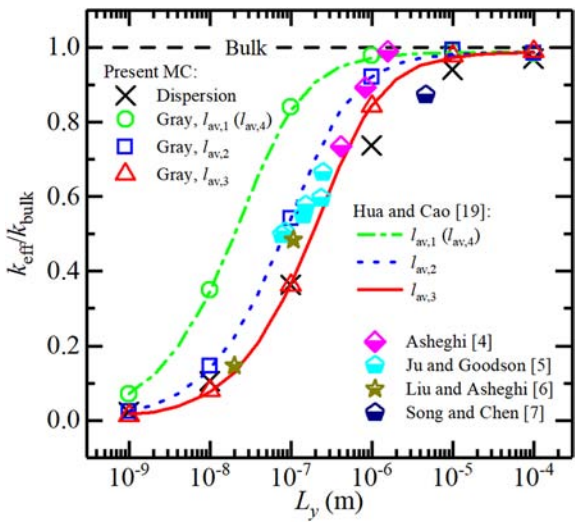

Fig. 4 Effective thermal conductivity varying with the lateral length (L_y) in in-plane heat conduction. The model comes from Ref. [19], and the experimetal data are extracted from Asheghi et al. [4]; Ju and Goodson [5]; Liu and Asheghi [6]; Song and Chen [7].

3.2 In-Plane Heat Conduction. The effective thermal conductivities simulated by the dispersion and gray medium MC simulations in in-plane heat conduction are depicted in Fig. 4, in which the predictions of a theoretical model [19] based on analytically solving gray medium BTE are illustrated too. The major concern of the in-plane heat conduction is the interactions between phonons and the lateral adiabatic walls, so the value of L_x is set to be 1×10^{-4} m in MC simulations to eliminate the x-directional size effect, and the lateral boundary conditions are set as diffusive reflection to generate obvious boundary heat flux slip. As well as decreasing L in the cross-plane case, decreasing L_y in the in-plane case leads to the reduction of the effective thermal conductivity, which varies from the bulk material value at $L_y = 100\,\mu$m to nearly zero at $L_y = 1$ nm. For the intermediate length scales, the difference between the simulation results has the same trend with Fig. 2, that is, gray medium approximation with $l_{av,3}$ has the minimum difference with phonon dispersion, and the difference increases for $l_{av,2}$ and reaches its maximum when using $l_{av,1}$ ($l_{av,4}$). Gray medium model with $l_{av,3}$ is also capable of approximating the results of dispersion MC, as the solid line has a favorable agreement with the cross symbols in Fig. 4. Moreover, for in-plane heat conduction, more experimental measurements of the thermal conductivity [4–7] can be found and their results are shown in Fig. 4. In general, our MC results by dispersion or $l_{av,3}$ are somewhat lower than these experimental data, while the results by $l_{av,2}$ are higher. The quantitative difference between present dispersion MC and the experimental data may be related to the diffusive lateral boundary, but it does not affect the comparison of the gray medium approximation and phonon dispersion.

Furthermore, detailed heat flux distributions of the MC simulation and the model are shown in Fig. 5, in which some insets show the enlarged figures of the bottom regions. The model always has an excellent consistency with the gray medium MC using the same average MFP. Compared to the dispersion MC, the gray medium simulation and model are able to qualitatively reflect the reduced heat flux near the boundaries who intensifies with the lateral length decreasing, but as expected, the value of the average MFP has a decisive role on the quantitative accuracy. For $L_y = 100\,\mu$m, all heat flux profiles are close to the vertical line predicted by Fourier's law, except for the results of dispersion MC in which a slight boundary heat flux slip takes place, as the enlarged figure in Fig. 5(*a*) shows. With L_y decreasing, the dimensionless heat fluxes near to the boundaries in every MC simulation start to get less than 1. The most remarkable slip effect is predicted by dispersion MC, which can be approached by gray MC using $l_{av,3}$. The gray simulation based on $l_{av,2}$ departs from the dispersion one, and the departure is even more for the simulation based on $l_{av,1}$ ($l_{av,4}$). For instance, when $L_y = 100$ nm, the values of the heat fluxes predicted by dispersion MC or gray MC with $l_{av,3}$ roughly lie between 0.3 and 0.4, while the range is about 0.5–0.6 and 0.7–0.9 for the gray MC using $l_{av,2}$ and $l_{av,1}$ ($l_{av,4}$), respectively. It is the enhancement of phonon boundary scattering that causes the dimensionless heat fluxes be lower than 1 everywhere in the film. When L_y further decreases to 1 nm, the phonon boundary scattering is so strong that all simulated results come

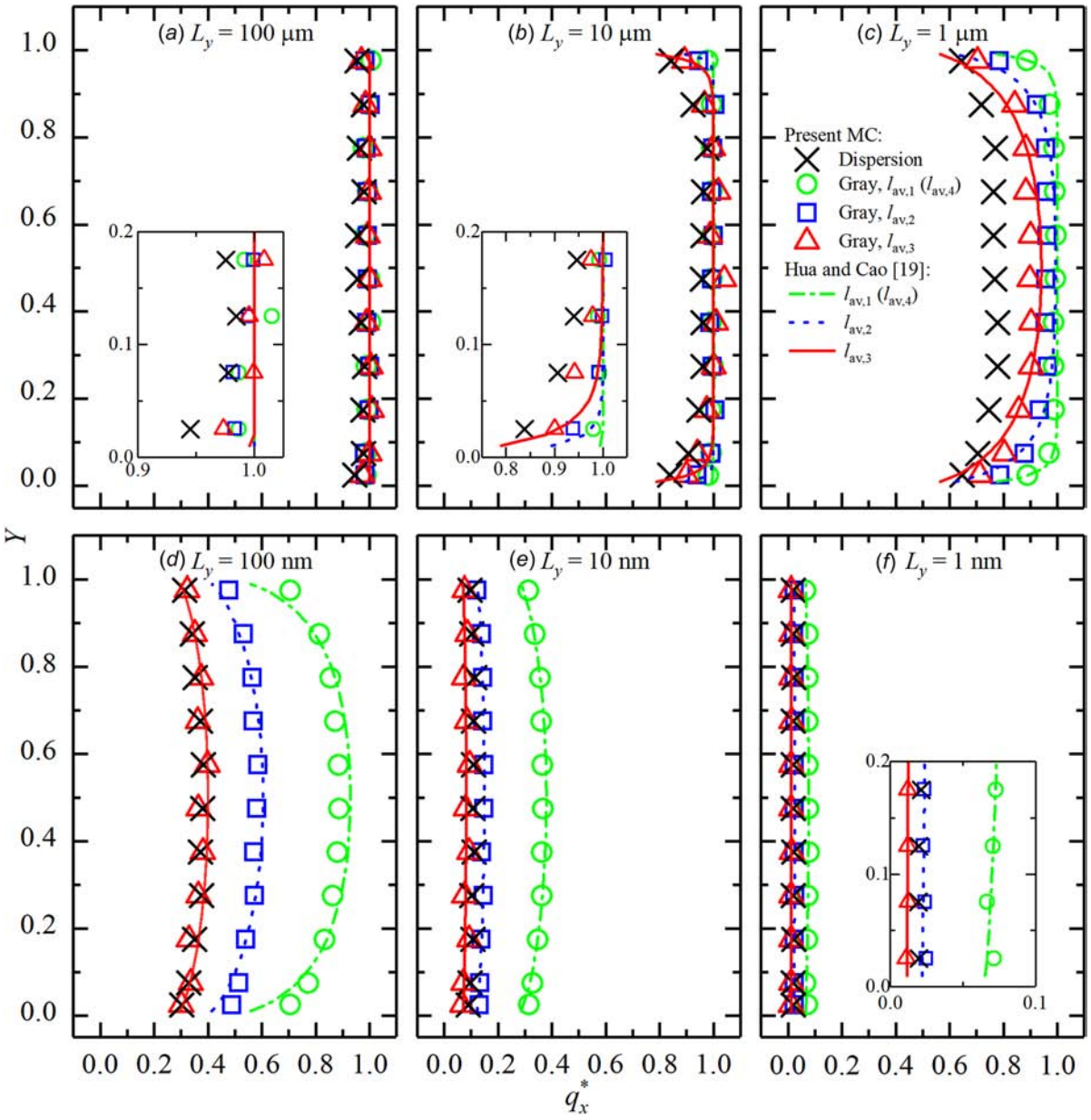

Fig. 5 Heat flux distribution varying with the lateral length (L_y) in in-plane heat conduction. The model comes from Ref. [19], and the insets show the enlarged figures of the bottom boundary for some dense results.

near to the ballistic limit value (0). Although the value of $l_{av,3}$ is calculated on account of the size effect in cross-plane heat conduction, it still performs better than other values in predicting the effective thermal conductivity and the heat flux distribution in the in-plane case. The results of in-plane heat conduction validate previous analyses about the accuracy of the four ways to calculate the average MFP.

4 Conclusions

We use phonon MC method to compare the use of gray medium approximation and phonon dispersion in ballistic-diffusive heat conduction of silicon films. By taking the results considering phonon dispersion as a benchmark, four different approaches to calculate the average MFP with the gray medium approximation are studied, which are: (1) the kinetic theory that uses Debye's theory to predict the specific heat and average group velocity ($l_{av,1}$); (2) the weighted average of the modal MFPs where the weighting coefficient is the product of the modal specific heat and group velocity ($l_{av,2}$); (3) extracting the average MFP from the fitting of the size-dependent effective thermal conductivity by a gray medium model ($l_{av,3}$); and (4) the inverse of the weighted average phonon emissivity ($l_{av,4}$). The first three methods can be classified as being based on the weighted average of the MFPs, while the last one is based on the weighted average of the reciprocals of the MFPs.

These methods are found to have different limitations. $l_{av,1}$ underestimates the average MFP since the specific heat and the average group velocity in Debye's model are unrealistically high for heat conduction. Dealing with phonon dispersion more carefully, $l_{av,2}$ ought to be more reasonable and accurate, but it still fails in predicting the size-dependent contribution of each phonon mode to the thermal conductivity. As an improvement, $l_{av,3}$ accurately reflects the reduction of the thermal conductivity and the heat flux on all scales, but its accuracy in calculating the temperature distribution is the worst. For $l_{av,4}$, the performance is just the reverse, namely, it obtains the most accurate temperature distribution at the sacrifice of the thermal conductivity and the heat flux distribution.

The failure to find a representative and robust average MFP is caused by the drawback of the gray medium approximation. By

lumping all phonons together, the gray medium approximation cannot simultaneously take the contribution of different phonon modes to the heat flux and the emitted power density into consideration, resulting in the tradeoff between the accuracy of the cross section-related thermal properties (the effective thermal conductivity and the heat flux distribution) and that of the volume-related thermal property (the equivalent equilibrium temperature). Accurate predictions of ballistic-diffusive heat conduction must take into account phonon dispersion.

Funding Data

- National Natural Science Foundation of China (Grant Nos. 51825601, 51676108, 51621062; Funder ID: 10.13039/501100001809).

Nomenclature

a = lattice constant
BTE = Boltzmann transport equation
C = volumetric specific heat capacity
D = volumetric density of state
e = energy distribution function
f = phonon distribution function
f^0 = Bose–Einstein distribution
k = thermal conductivity
Kn = Knudsen number
l = phonon mean-free-path
L = characteristic length of the system
l_{av} = average phonon mean-free-path
MC = Monte Carlo
T = temperature
v = phonon group velocity
ε = phonon absorption coefficient
τ = phonon relaxation time
ω = phonon angular frequency

References

[1] Allu, P., and Mazumder, S., 2016, "Hybrid Ballistic-Diffusive Solution to the Frequency-Dependent Phonon Boltzmann Transport Equation," Int. J. Heat Mass Transf., **100**, pp. 165–177.
[2] Hanks, D. F., Lu, Z., Sircar, J., Salamon, T. R., Antao, D. S., Bagnall, K. R., Barabadi, B., and Wang, E. N., 2018, "Nanoporous Membrane Device for Ultra High Heat Flux Thermal Management," Microsyst. Nanoeng., **4**(1), pp. 1–10.
[3] Moore, A. L., and Shi, L., 2014, "Emerging Challenges and Materials for Thermal Management of Electronics," Mater. Today, **17**(4), pp. 163–174.
[4] Asheghi, M., Leung, Y. K., Wong, S. S., and Goodson, K. E., 1997, "Phonon-Boundary Scattering in Thin Silicon Layers," Appl. Phys. Lett., **71**(13), pp. 1798–1800.
[5] Ju, Y. S., and Goodson, K. E., 1999, "Phonon Scattering in Silicon Films With Thickness of Order 100 nm," Appl. Phys. Lett., **74**(20), pp. 3005–3007.
[6] Liu, W., and Asheghi, M., 2004, "Phonon-Boundary Scattering in Ultrathin Single-Crystal Silicon Layers," Appl. Phys. Lett., **84**(19), pp. 3819–3821.
[7] Song, D., and Chen, G., 2004, "Thermal Conductivity of Periodic Microporous Silicon Films," Appl. Phys. Lett., **84**(5), pp. 687–689.
[8] Hopkins, P. E., Reinke, C. M., Su, M. F., Olsson, R. H., Shaner, E. A., Leseman, Z. C., Serrano, J. R., Phinney, L. M., and El-Kady, I., 2011, "Reduction in the Thermal Conductivity of Single Crystalline Silicon by Phononic Crystal Patterning," Nano Lett., **11**(1), pp. 107–112.
[9] Maznev, A. A., Cuffe, J., Eliason, J. K., Minnich, A. J., Kehoe, T., Torres, C. M. S., Chen, G., Nelson, K. A., and Johnson, J. A., 2013, "Direct Measurement of Room-Temperature Nondiffusive Thermal Transport Over Micron Distances in a Silicon Membrane," Phys. Rev. Lett., **110**(2), p. 025901.
[10] Maire, J., Anufriev, R., Hori, T., Shiomi, J., Volz, S., and Nomura, M., 2018, "Thermal Conductivity Reduction in Silicon Fishbone Nanowires," Sci. Rep., **8**(1), p. 4452.
[11] Volz, S., Shiomi, J., Nomura, M., and Miyazaki, K., 2016, "Heat Conduction in Nanostructured Materials," J. Therm. Sci. Tech., **11**(1), p. JTST0001.
[12] Bao, H., Chen, J., Gu, X. K., and Cao, B. Y., 2018, "A Review of Simulation Methods in Micro/Nanoscale Heat Conduction," ES Energy Environ., **1**, pp. 16–55.
[13] Chen, G., 1998, "Thermal Conductivity and Ballistic-Phonon Transport in the Cross-Plane Direction of Superlattices," Phys. Rev. B, **57**(23), pp. 14958–14973.
[14] Chen, G., 2001, "Ballistic-Diffusive Heat-Conduction Equations," Phys. Rev. Lett., **86**(11), pp. 2297–2300.
[15] Alvarez, F. X., and Jou, D., 2010, "Boundary Conditions and Evolution of Ballistic Heat Transport," ASME J. Heat Transfer, **132**(1), p. 012404.
[16] Li, B. W., and Wang, J., 2003, "Anomalous Heat Conduction and Anomalous Diffusion in One-Dimensional Systems," Phys. Rev. Lett., **91**(4), p. 044301.
[17] Sellan, D. P., Turney, J. E., McGaughey, A. J. H., and Amon, C. H., 2010, "Cross-Plane Phonon Transport in Thin Films," J. Appl. Phys., **108**(11), p. 113524.
[18] Aoki, K., and Kusnezov, D., 2001, "Fermi-Pasta-Ulam Beta Model: Boundary Jumps, Fourier's Law, and Scaling," Phys. Rev. Lett., **86**(18), pp. 4029–4032.
[19] Hua, Y. C., and Cao, B. Y., 2017, "Slip Boundary Conditions in Ballistic-Diffusive Heat Transport in Nanostructures," Nanoscale Microscale Thermophys. Eng., **21**(3), pp. 159–176.
[20] Li, H. L., Hua, Y. C., and Cao, B. Y., 2018, "A Hybrid Phonon Monte Carlo-Diffusion Method for Ballistic-Diffusive Heat Conduction in Nano- and Micro-Structures," Int. J. Heat Mass Transfer, **127**, pp. 1014–1022.
[21] Parrish, K. D., Abel, J. R., Jain, A., Malen, J. A., and McGaughey, A. J., 2017, "Phonon-Boundary Scattering in Nanoporous Silicon Films: Comparison of Monte Carlo Techniques," J. Appl. Phys., **122**(12), p. 125101.
[22] Liu, W., Etessam-Yazdani, K., Hussin, R., and Asheghi, M., 2006, "Modeling and Data for Thermal Conductivity of Ultrathin Single-Crystal SOI Layers at High Temperature," IEEE T. Electron Dev., **53**(8), pp. 1868–1876.
[23] Chung, J. D., Mcgaughey, A. J. H., and Kaviany, M., 2004, "Role of Phonon Dispersion in Lattice Thermal Conductivity Modeling," ASME J. Heat Transfer, **126**(3), pp. 376–380.
[24] Baillis, D., and Randrianalisoa, J., 2009, "Prediction of Thermal Conductivity of Nanostructures: Influence of Phonon Dispersion Approximation," Int. J. Heat Mass Transfer, **52**(11–12), pp. 2516–2527.
[25] Jeong, C., Datta, S., and Lundstrom, M., 2011, "Full Dispersion Versus Debye Model Evaluation of Lattice Thermal Conductivity With a Landauer Approach," J. Appl. Phys., **109**(7), p. 073718.
[26] Mazumder, S., and Majumdar, A., 2001, "Monte Carlo Study of Phonon Transport in Solid Thin Films Including Dispersion and Polarization," ASME J. Heat Transfer, **123**(4), pp. 749–759.
[27] Lacroix, D., Joulain, K., and Lemonnier, D., 2005, "Monte Carlo Transient Phonon Transport in Silicon and Germanium at Nanoscales," Phys. Rev. B, **72**(6), p. 064305.
[28] Jeng, M., Yang, R., Song, D., and Chen, G., 2008, "Modeling the Thermal Conductivity and Phonon Transport in Nanoparticle Composites Using Monte Carlo Simulation," ASME J. Heat Transfer, **130**(4), p. 042410.
[29] Hao, Q., Chen, G., and Jeng, M. S., 2009, "Frequency-Dependent Monte Carlo Simulations of Phonon Transport in Two-Dimensional Porous Silicon With Aligned Pores," J. Appl. Phys., **106**(11), p. 114321.
[30] Péraud, J.-P. M., and Hadjiconstantinou, N. G., 2011, "Efficient Simulation of Multidimensional Phonon Transport Using Energy-Based Variance-Reduced Monte Carlo Formulations," Phys. Rev. B, **84**(20), pp. 1555–1569.
[31] Péraud, J.-P. M., and Hadjiconstantinou, N. G., 2012, "An Alternative Approach to Efficient Simulation of Micro/Nanoscale Phonon Transport," Appl. Phys. Lett., **101**(15), p. 153114.
[32] Hori, T., Chen, G., and Shiomi, J., 2014, "Thermal Conductivity of Bulk Nanostructured Lead Telluride," Appl. Phys. Lett., **104**(2), p. 021915.
[33] Zeng, L., Collins, K. C., Hu, Y., Luckyanova, M. N., Maznev, A. A., Huberman, S., Chiloyan, V., Zhou, J., Huang, X., Nelson, K. A., and Chen, G., 2015, "Measuring Phonon Mean Free Path Distributions by Probing Quasiballistic Phonon Transport in Grating Nanostructures," Sci. Rep., **5**, p. 17131.
[34] Hu, Y., Zeng, L., Minnich, A. J., Dresselhaus, M. S., and Chen, G., 2015, "Spectral Mapping of Thermal Conductivity Through Nanoscale Ballistic Transport," Nat. Nanotechnol., **10**(8), pp. 701–706.
[35] Jiang, P. Q., Lindsay, L., and Koh, Y. K., 2016, "Role of Low-Energy Phonons With Mean-Free-Paths >0.8 μm in Heat Conduction in Silicon," J. Appl. Phys., **119**(24), p. 245705.
[36] Majumdar, A., 1993, "Microscale Heat Conduction in Dielectric Thin Films," ASME J. Heat Transfer, **115**(1), pp. 7–16.
[37] Alvarez, F. X., and Jou, D., 2007, "Memory and Nonlocal Effects in Heat Transport: From Diffusive to Ballistic Regimes," Appl. Phys. Lett., **90**(8), p. 083109.
[38] Hua, Y. C., and Cao, B. Y., 2016, "Ballistic-Diffusive Heat Conduction in Multiply-Constrained Nanostructures," Int. J. Therm. Sci., **101**, pp. 126–132.
[39] Hua, Y. C., and Cao, B. Y., 2016, "The Effective Thermal Conductivity of Ballistic-Diffusive Heat Conduction in Nanostructures With Internal Heat Source," Int. J. Heat Mass Transf., **92**, pp. 995–1003.
[40] Hua, Y. C., and Cao, B. Y., 2017, "Cross-Plane Heat Conduction in Nanoporous Silicon Thin Films by Phonon Boltzmann Transport Equation and Monte Carlo Simulations," Appl. Therm. Eng., **111**, pp. 1401–1408.
[41] Li, H. L., and Cao, B. Y., 2019, "Radial Ballistic-Diffusive Heat Conduction in Nanoscale," Nanoscale Microscale Thermophys. Eng., **23**(1), pp. 10–24.
[42] Lepri, S., Livi, R., and Politi, A., 2003, "Thermal Conduction in Classical Low-Dimensional Lattices," Phys. Rep., **377**(1), pp. 1–80.
[43] Hua, Y. C., and Cao, B. Y., 2014, "Phonon Ballistic-Diffusive Heat Conduction in Silicon Nanofilms by Monte Carlo Simulations," Int. J. Heat Mass Transf., **78**, pp. 755–759.
[44] Maassen, J., and Lundstrom, M., 2015, "Steady-State Heat Transport: Ballistic-to-Diffusive With Fourier's Law," J. Appl. Phys., **117**(3), p. 011305.
[45] Sobolev, S. L., 2017, "Discrete Space-Time Model for Heat Conduction: Application to Size- Dependent Thermal Conductivity in Nano-Films," Int. J. Heat Mass Transf., **108**, pp. 933–939.
[46] Kaiser, J., Feng, T., Maassen, J., Wang, X., Ruan, X., and Lundstrom, M., 2017, "Thermal Transport at the Nanoscale—A Fourier's Law vs. Phonon Boltzmann Equation Study," J. Appl. Phys., **121**(4), p. 044302.
[47] Chen, G., 2005, "Nanoscale Energy Transport and Conversion: A Parallel Treatment of Electrons," *Molecules, Phonons, and Photons*, Oxford University Press, New York.
[48] Narumanchi, S. V. J., Murthy, J. Y., and Amon, C. H., 2006, "Boltzmann Transport Equation-Based Thermal Modeling Approaches for Hotspots in Microelectronics," Heat Mass Transf., **42**(6), pp. 478–491.

[49] Vallabhaneni, A. K., Chen, L., Gupta, M. P., and Kumar, S., 2017, "Solving Nongray Boltzmann Transport Equation in Gallium Nitride," ASME J. Heat Transfer, **139**(10), p. 102701.
[50] Cahill, D. G., Braun, P. V., Chen, G., Clarke, D. R., Fan, S., Goodson, K. E., Keblinski, P., King, W. P., Mahan, G. D., Majumdar, A., Maris, H. J., Phillpot, S. R., Pop, E., and Shi, L., 2014, "Nanoscale Thermal Transport—II: 2003–2012," Appl. Phys. Rev., **1**(1), p. 011305.
[51] Sobolev, S. L., 2018, "Hyperbolic Heat Conduction, Effective Temperature, and Third Law for Nonequilibrium Systems With Heat Flux," Phys. Rev. E, **97**(2), p. 022122.
[52] Peterson, R. B., 1994, "Direct Simulation of Phonon-Mediated Heat Transfer in a Debye Crystal," ASME J. Heat Transfer, **116**(4), pp. 815–822.
[53] Murthy, J. Y., and Mathur, S. R., 2002, "Computation of Sub-Micron Thermal Transport Using an Unstructured Finite Volume Method," ASME J. Heat Transfer, **124**(6), pp. 1176–1181.
[54] Brockhouse, B. N., 1959, "Lattice Vibrations in Silicon and Germanium," Phys. Rev. Lett., **2**(6), pp. 256–258.
[55] Esfarjani, K., Chen, G., and Stokes, H. T., 2011, "Heat Transport in Silicon From First Principles Calculations," Phys. Rev. B, **84**(8), pp. 293–293.
[56] Holland, M. G., 1963, "Analysis of Lattice Thermal Conductivity," Phys. Rev., **132**(6), pp. 2461–2471.
[57] Kukita, K., and Kamakura, Y., 2013, "Monte Carlo Simulation of Phonon Transport in Silicon Including a Realistic Dispersion Relation," J. Appl. Phys., **114**(15), p. 154312.
[58] Chen, G., 1997, "Size and Interface Effects on Thermal Conductivity of Superlattices and Periodic Thin-Film Structures," ASME J. Heat Transfer, **119**(2), pp. 220–229.
[59] Pohl, R. O., and Swartz, E. T., 1989, "Thermal Boundary Resistance," Rev. Mod. Phys., **61**(3), pp. 605–668.